Compact Parameterized Black-Box Modeling via Fourier-Rational Approximations

Compact Parameterized Black-Box Modeling via Fourier-Rational Approximations

Stefano Grivet-Talocia, *Senior Member, IEEE*, Elisa Fevola

***Abstract*—We present a novel black-box modeling approach for frequency responses that depend on additional parameters with periodic behavior. The methodology is appropriate for representing with compact, low-order equivalent models the behavior of electromagnetic systems observed at well-defined ports and/or locations, including dependence on geometrical parameters with rotational symmetry. Examples can be polarization or incidence angles of a plane wave, or stirrer rotation in reverberation chambers. The proposed approach is based on fitting a Fourier-rational model to sampled frequency responses, where frequency dependence is represented through rational functions and parameter dependence through a Fourier series. Several examples from different applications are used to validate and demonstrate the approach.**

***Index Terms*—Macromodeling, parameterized modeling, transmission lines, field coupling, rational approximation, reduced order modeling, Vector Fitting.**

I. Introduction and Motivation

Accurate and compact models of complex physical phenomena or processes are often required in EMC applications [5], [6], as well as in several other engineering disciplines [3], [4]. Full numerical modeling from first-principle descriptions, like solving Maxwell's equations at the system level, is sometimes impractical due to the overwhelming complexity, both in electrical size (leading to an excessive number of unknowns to be solved for) and other factors like, e.g., the presence of nonlinearities in the system (which prevent using a direct frequency-domain modeling approach). In such situations, a common approach is to break this complexity by performing a system partitioning or domain decomposition, modeling each individual subsystem using the most appropriate method, and then combining the results for a system-level characterization [25], [30], [31].

This paper addresses the problem of constructing behavioral models starting from tabulated frequency responses, as may be obtained by a frequency-domain full-wave simulation or by a VNA measurement. Several algorithms are available for this task and are widely used by the EMC community, including the well-known Vector Fitting (VF) scheme [7]–[10] and, to a lesser extent, the Loewner framework [3], [11]. A complete overview on the state of the art of theory and applications can be found in [1]. These approaches process the frequency samples (usually in form of Scattering parameters) and produce a lumped model in state-space form. The latter can be readily synthesized as a SPICE netlist for circuit simulation [12], [13]. Model construction automatically performs an order reduction, by selecting the minimal complexity that is strictly required for the representation of the frequency response of interest. This approach is mature and widespred in both academia and industry.

The focus of this work is on the more general multivariate or parameterized modeling. In addition to reproducing the system response over a broad frequency band, we include in the model also the dependence on one additional variable or parameter. This approach is not new, since several algorithms for the construction of parameterized black-box models exist [19]–[23]. Practically all these prior works represent the variations induced by external parameters through low-degree polynomials, either full-domain or piecewise, thus limiting scope and applications.

In this work, we introduce a novel Fourier-rational model representation. Frequency dependence is represented through low-order rational functions, so that models are compatible with state-space descriptions and equivalent circuit synthesis. Parameter dependence is instead represented by a truncated Fourier series, which is appropriate for all those cases where the parameter is an angle or is characterized by a periodic behavior. Even when this periodicity assumption does not hold, the Fourier basis functions still provide excellent building blocks for all those cases that are characterized by a smooth parameter dependence over a finite range. In addition, it is well known that Fourier-based approximations are characterized by optimal numerical conditioning, differently from polynomials, whose application is instead limited to low orders.

Various different applications are discussed in this paper. First, we show that the model representation and the corresponding coefficient determination, based on a reformulation of the Sanathanan-Koerner iteration [24], allow a perfect identification in case the system under modeling has a finite dynamical order (a fixed number of poles), with a frequency response that, at any frequency, depends on the parameter through a finite number of harmonics. We use a simple lumped circuit as validation benchmark for this basic consistency check.

A second and more realistic application involves the representation of electromagnetic field coupling to transmission lines [26]. We show that, starting from either a transmission-line model or from frequency responses computed via a full-wave numerical simulation (thus including re-radiation and edge effects), the proposed approach results in compact models for loaded or unloaded lines, excited by an impinging plane wave and parameterized by the incidence or polarization angle. The final outcome is a parameter-dependent SPICE netlist, which can be used in a SPICE transient analysis by loading the model with nonlinear terminations. The suggested procedure

Manuscript received ...; revised ...

S. Grivet-Talocia and E. Fevola are with the Department of Electronics and Telecommunications, Politecnico di Torino, Torino 10129, Italy (e-mail: stefano.grivet@polito.it).

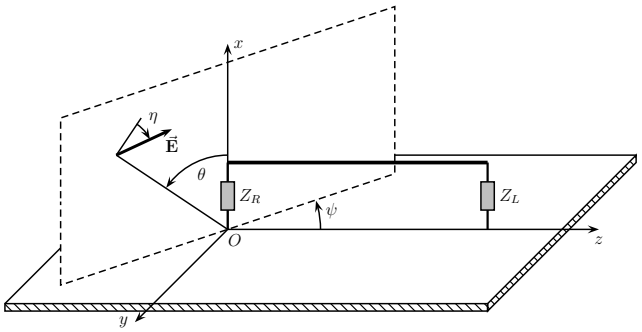

Fig. 1. A field-excited transmission line, with specification of polarization η and incidence angles (θ, ψ).

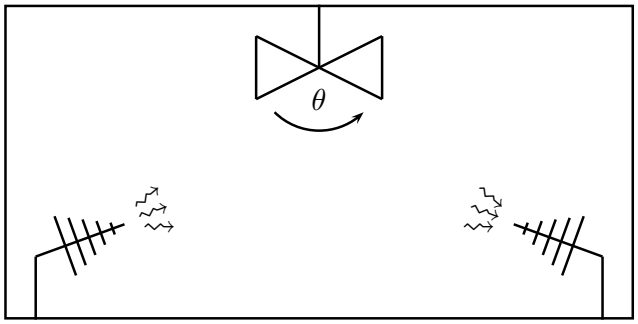

Fig. 2. A schematic illustration of a reverberation chamber, with specification of stirrer rotation angle θ.

thus enables fast simulation of field-excited transmission lines loaded by nonlinear elements. This example serves as a proof-of-concept for EMI modeling via compact behavioral models, whereas the passive interconnect macromodel is generalized to a Norton or Thévenin model having an equivalent source in Fourier-rational form and compatible with subsequent parameterized circuit simulation.

A third application that we demonstrate here is the blind identification of resonant modes in reverberation chambers starting from direct measurements, including a full representation of the mode dependence on the stirrer rotation angle. Opposed to more standard repeated mode identification for fixed angles [2], [28], [29], the proposed approach allows a continuous mode-tracking with stirrer rotation, thus allowing more realistic chamber characterization and subsequent statistical analysis.

In this work, we focus on the model representation and on the performance of the coefficient identification algorithm. We do not discuss important related topics, such as uniform model passivity characterization and enforcement [14]–[18], which are left for a future investigation.

II. Problem statement

Let us consider the two application scenarios depicted in Figures 1 and 2. Figure 1 reports a simple transmission line over a ground plane, loaded by two impedances Z_R and Z_L, and excited by a plane wave with incidence and polarization defined by the triplet of angles (θ, ψ, η). The quantity of interest is here the current induced on one of the terminations, i.e., Z_L. This current will depend on frequency (time) and on the three incidence angles as $I_L(s; \theta, \psi, \eta)$, where s is the Laplace variable.

Figure 2 depicts instead an idealized reverberation chamber, excited by an antenna whose feed is denoted as "port 1", and whose field is measured by a second antenna ("port 2"). The quantity of interest here is the scattering matrix $\mathbf{S}$ that represents energy reflection and transmission between the two ports, which is parameterized by the stirrer rotation angle θ. The resulting parameterization can thus be written in the frequency (Laplace) domain as $\mathbf{S}(s; \theta)$.

The parameterized frequency responses in above two scenarios will be collectively denoted in the following as $\breve{\mathbf{H}}(s; \vartheta)$, where the accent $\breve{}$ will be used to label the original or "true" system responses, and where ϑ represents a generic parameter with periodic behavior within the range $[\vartheta_{\min}, \vartheta_{\max}]$. When ϑ is an angle, $\vartheta_{\min} = 0^o$ and $\vartheta_{\max} = 360^o$ (this will be implicitly assumed in the following). In general, $\breve{\mathbf{H}}$ is a $P \times Q$ matrix-valued response.

The "true" response can be reasonably evaluated at a set of fixed frequencies $f_k,\ k = 1, \ldots, K$ over a given frequency band $[f_{\min}, f_{\max}]$, with $f_1 = f_{\min}$ and $f_K = f_{\max}$, and for a set of fixed parameter values $\vartheta_m,\ m = 1, \ldots, M$ spanning the range $[\vartheta_{\min}, \vartheta_{\max}]$. We will denote this characterization as

$$\breve{\mathbf{H}}_{k;m} = \breve{\mathbf{H}}(\mathrm{j}2\pi f_k; \vartheta_m), \quad k = 1, \ldots, K,\ m = 1, \ldots, M. \tag{1}$$

The evaluation of this data can be performed by a direct measurement (as in the reverberation chamber example), or by a numerical simulation (as in the trasmission-line example). The parameterized model to be constructed will be denoted as $\mathbf{H}(s; \vartheta)$. We will enforce the following fitting condition

$$\mathbf{H}(\mathrm{j}2\pi f_k; \vartheta_m) \approx \breve{\mathbf{H}}_{k;m}, \quad k = 1, \ldots, K,\ m = 1, \ldots, M \tag{2}$$

so that the model responses approximate the raw data throughout the modeling bandwidth and parameter range.

We remark that the proposed approach is not limited to the above two examples, which were chosen for illustration purposes. Any linear dynamic system with periodically-varying parameters can be analyzed.

III. Fourier-rational model structure

The structure of the model to be constructed is determined based on the following considerations:

1) given the periodicity assumptions, for any complex frequency s, the elements of matrix $\mathbf{H}(s; \vartheta)$ should be periodic functions of ϑ;
2) for any parameter value ϑ, the elements of matrix $\mathbf{H}(s; \vartheta)$ should be rational functions of the complex frequency s;
3) in order to ensure generality, both poles and zeros (or equivalently poles and residues) of $\mathbf{H}(s; \vartheta)$ should depend on the variable ϑ;
4) the parameterization of the poles $p(\vartheta)$ and zeros $z(\vartheta)$ should not be explicit but implicit, since $p(\vartheta)$ and $z(\vartheta)$ may undergo bifurcations induced by variations of ϑ, resulting in a non-smooth behavior (such an example is reported in the Appendix);

5) following the above point, the model parameterization should be based on smooth functions of ϑ.

We introduce the following Fourier-rational form

$$\mathbf{H}(s;\vartheta)=\frac{\mathbf{N}(s,\vartheta)}{\mathsf{D}(s,\vartheta)}=\frac{\displaystyle\sum_{\ell=0}^{2L}\sum_{n=0}^{N}\mathbf{C}_{\ell,n}\xi_\ell(\vartheta)\varphi_n(s)}{\displaystyle\sum_{\ell=0}^{2L}\sum_{n=0}^{N}d_{\ell,n}\xi_\ell(\vartheta)\varphi_n(s)} \tag{3}$$

where the parameter-dependent basis functions are defined as the Fourier basis in trigonometric form

$$\xi_\ell(\vartheta)=\begin{cases}1 & \ell=0\\ \cos(\lceil\ell/2\rceil\vartheta) & \ell=1,3,5,\dots\\ \sin(\lceil\ell/2\rceil\vartheta) & \ell=2,4,6,\dots\end{cases} \tag{4}$$

where operator $\lceil\cdot\rceil$ rounds its argument to the nearest larger integer. The frequency-dependent basis functions are instead defined as the partial fractions

$$\varphi(s)=\begin{cases}1 & n=0\\ (s-q_n)^{-1} & n>0\end{cases} \tag{5}$$

where the set $\mathcal{Q}=\{q_n,\ n=1,\dots,N\}$ includes N prescribed and distinct numbers (real or complex conjugate pairs). In order to guarantee uniqueness in the model representation, we normalize the model by setting $d_{0,0}=1$.

A few remarks are in order. The adopted model structure in its general form (3) is the same as discussed in [1] and originally postulated in [20]–[23], where polynomials or piecewise polynomials were used as basis functions ξ_ℓ. The main novelty that is introduced in this work is the Fourier basis to represent periodic variations. Surprisingly, and to the best of Authors' knowledge, this representation was never proposed before. We also note that, once all coefficients in (3) are known, a state-space form providing a model realization, and an associated SPICE netlist providing a circuit realization are readily constructed, as discussed in [1], [20]. We omit these details here, pointing the Reader to the cited references.

The proposed Fourier basis is appropriate when the dependence of the coefficients on the parameters is expected or known to be smooth (point 5 above). Should this assumption not be true, spurious oscillations and Gibbs phenomena may appear in the neighborhood of some point ϑ_* where either numerator or denominator of (3) has a singularity in some of its derivatives. In such cases, it would be more appropriate to use piecewise-defined Finite-Element-like bases. This investigation is however out of scope for this work.

IV. Model identification

Following the standard procedure discussed in [1], [20], [24], model identification is performed here using a linear relaxation of the fitting condition (2), known as (Generalized) Sanathanan-Koerner (GSK) iteration. In fact, a direct nonlinear optimization applied to (2) would result in a very difficult numerical problem, since the cost function expressing the fitting error (based on the energy norm)

$$E=\sum_{k=1}^{K}\sum_{m=1}^{M}\left\|\mathbf{H}(\mathrm{j}2\pi f_k;\vartheta_m)-\breve{\mathbf{H}}_{k;m}\right\|^2 \tag{6}$$

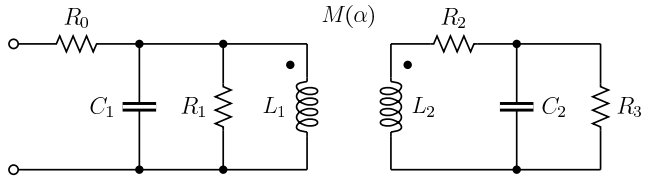

Fig. 3. Circuit schematic used for validation. Parameter values are: $R_0=R_2=1\,\Omega$, $R_1=R_3=100\,\mathrm{k}\Omega$, $L_1=L_2=0.1\,\mathrm{mH}$, $C_1=C_2=0.1\,\mu\mathrm{F}$; see text for $M(\alpha)$.

is strongly non-convex in the decision variables $\mathbf{C}_{\ell,n}, d_{\ell,n}$. For this class of problems, the SK iteration has proven an excellent identification method, although its theoretical convergence properties are still partially unknown and under debate [38], [39].

We setup an iterative scheme indexed by $\mu=0,1,2,\dots$, and we minimize at each iteration the cost function

$$J^\mu=\sum_{k=1}^{K}\sum_{m=1}^{M}\frac{\left\|\mathbf{N}^\mu(\mathrm{j}2\pi f_k;\vartheta_m)-\mathsf{D}^\mu(\mathrm{j}2\pi f_k;\vartheta_m)\breve{\mathbf{H}}_{k;m}\right\|^2}{\left|\mathsf{D}^{\mu-1}(\mathrm{j}2\pi f_k;\vartheta_m)\right|^2} \tag{7}$$

for $\mu=1,2,\dots$, with the initialization $\mathsf{D}^0=1$. The minimization of (7) does not pose particular problems, since all decision variables appear as a linear combination in the numerator expression (the denominator is known, since based on the solution at previous iteration). This is recognized as a weighted linear least squares problem, for which the optimal solution is found using standard linear algebra tools. We also remark that, when iterations stabilize, we have $\mathsf{D}^\mu=\mathsf{D}^{\mu-1}$, and J^μ becomes identical to E in (6). The iterations are run until the value of the cost function J^μ stabilizes. If this value is below a prescribed threshold ε, the model is accepted and the iterations stop. Otherwise, the model order is increased and the identification restarted.

The above SK iteration is not able to enforce model stability and passivity by construction. In fact, the proposed model parameterization is global and not of interpolatory nature, therefore passive (and stable) interpolation schemes such as [21]–[23] cannot be used. To the best of Authors' knowledge, there is no general result for controlling or imposing uniform stability and passivity, so that this remains a clear objective for future investigations. However, both stability and passivity can be easily verified a posteriori, by performing a parameter sweep of the model response and checking stability and passivity of the corresponding univariate (non-parameterized) frequency-dependent models instantiated for fixed parameter values. This is the approach that was adopted in this work to certify the extracted macromodels as appropriate for stable time-domain analysis.

V. Validation

The proposed model formulation and identification algorithm are validated using the template one-port circuit depicted in Fig. 3. The circuit response (we consider the reflection coefficient $\Gamma^{\mathrm{in}}=S_{11}$) is parameterized by $\alpha\in[0^o,360^o]$ through the mutual inductance $M(\alpha)=\sqrt{L_1L_2}\,k(\alpha)$, where $k(\alpha)$ is a parameter-dependent coupling coefficient. This simple circuit

is an idealized model of two rotating windings, parameterized by the rotation angle. We consider the following two different scenarios.

- **finite harmonics:** we define the coupling coefficient as

$$k(\alpha) = [\kappa_1 \cos(\alpha) + \kappa_2 \cos(3\alpha)] \tag{8}$$

with $\kappa_{1,2}$ constants, corresponding to a finite number of harmonics in its Fourier representation. A straightforward analytic circuit solution shows that both numerator and denominator of $\Gamma^{\text{in}}(s;\alpha)$ include a finite terms of Fourier basis functions (4), up to $2L = 12$. This implies that fitting a parameteric model with $2L \geq 12$ should lead to an exact identification, within machine precision.
- **infinite harmonics:** we define the coupling coefficient as

$$\hat{k}(\alpha) = \mathcal{T}(k(\alpha)), \tag{9}$$

where the nonlinear function

$$\mathcal{T}(x) = \frac{1}{2}\left[\tanh\left(\frac{x-1/2}{\tau}\right) + \tanh\left(\frac{x+1/2}{\tau}\right)\right] \tag{10}$$

is used to generate an infinite number of harmonics in its Fourier representation and, consequently, in $\Gamma^{\text{in}}(s;\alpha)$.

The finite and infinite harmonics cases were analyzed by generating the exact responses $\breve{\Gamma}^{\text{in}}_{k;m}$ over a grid of $K = 500$ logarithmically spaced frequency samples from 10 kHz to 1 MHz, and $M = 360$ samples along α with spacing of one degree. The SK identification was then run with different orders, in order to investigate consistency and convergence. Top and bottom panels of Fig. 4 depict the model identification (relative) errors achieved for the finite and infinite harmonics cases (top and bottom panels, respectively), for different values of the constants $\kappa_{1,2}$ and saturation coefficient τ. As expected, we see that in the finite harmonics case machine precision is reached with $2L = 12$ Fourier basis functions, for all different sub-cases (the order was increased in steps of 2, so that both the cosine and the sine terms are included in the basis for each harmonic). In the infinite harmonics case, instead, a larger number of harmonics is required to obtain engineering accuracy. For smaller τ, the error decay versus order is less sharp, consistently with the stronger saturation effects.

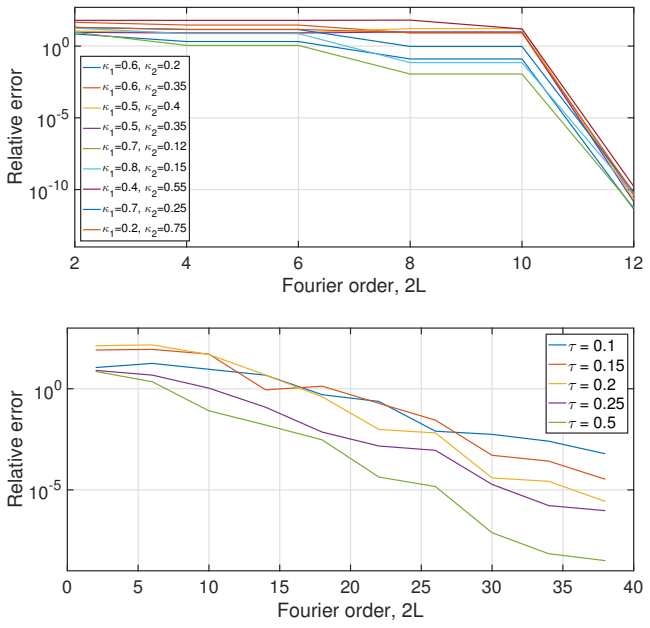

Fig. 4. Relative model errors in the finite (top) and infinite (bottom) harmonics cases (in the bottom panel, $\kappa_1 = 0.6$ and $\kappa_2 = 0.2$).

A summary of the main results for a few selected parameter configurations is depicted in Fig. 5. Each row in the figure corresponds to a given configuration (as labeled in the left graph). For each case, we report in the first column a comparison between (the real part of) the raw data $\breve{\Gamma}^{\text{in}}(s;\alpha)$ (blue lines) and the parameterized model $\Gamma^{\text{in}}(s;\alpha)$ (red dots), for a selected subset of parameter values α_m (similar results were obtained for all other angles). The two sets of curves are undistinguishable, thus perfectly validating the model. The second column reports the real part of $\breve{\Gamma}^{\text{in}}(s;\alpha)$ plotted versus frequency and α, with a color scale ranging from blue ($\Re\Gamma = -1$) to yellow ($\Re\Gamma = +1$). The superimposed blue lines correspond to the (postive) imaginary parts of the exact circuit poles, whereas the red dots correspond to the poles of the identified model. The poles trajectories are seen to closely follow the peaks of the frequency responses. A complete validation of all model poles in terms of both real and imaginary parts is shown in the right column, showing a perfect match even when the two system poles appear to be very close to each other (middle panels) in terms of their imaginary part.

VI. Field-Excited Interconnects

We now refer to the template field-excited interconnect depicted in Figure 1. Modeling field coupling to transmission lines is well understood and well established [26], [33]–[37]. Here, we use this example as a proof of concept for the feasibility of proposed parameterized modeling strategy, in view of the more general problem of EMI modeling of complex interconnect structures loaded by nonlinear terminations. A reference frequency-domain solution for the field-excited line is here obtained through a full-wave MoM formulation using the well-known solver NEC [27], although other transmission-line-based models can be adopted [26], [32]–[37].

The line geometry under analysis [32] includes a uniform circular wire of length $\mathcal{L} = 1$ m and radius $r_w = 0.1$ mm, placed at a height $h = 0.1$ m over an ideal ground plane, corresponding to a characteristic impedance $Z_C \simeq 456\ \Omega$. The wire is loaded by two impedances Z_R and Z_L. The quantity of interest is the current through impedance Z_L, which will be parameterized by frequency (up to 1 GHz in this study) and by one of the incidence ψ or polarization η angles. Throughout this section, we set $Z_R = Z_C/10$.

Our modeling approach is based on the derivation of a Norton equivalent of the distributed one-port obtained after removing the load impedance Z_L (see Figure 6). The Norton equivalent admittance Y_{eq} is obtained by computing the current through a unit voltage source applied to the output port, while switching off the incident field. Since the incident field is not present, this equivalent admittance is a univariate function

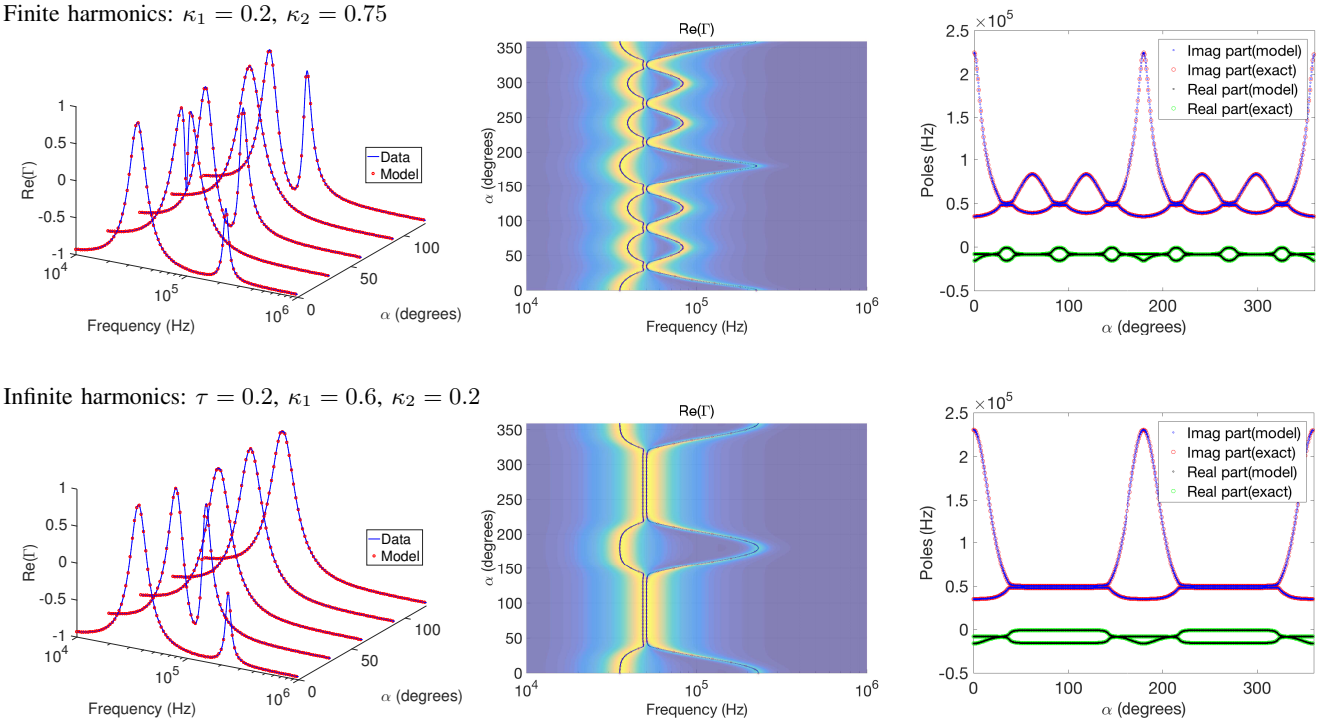

Fig. 5. Validation summary for two circuit configurations. See text for details.

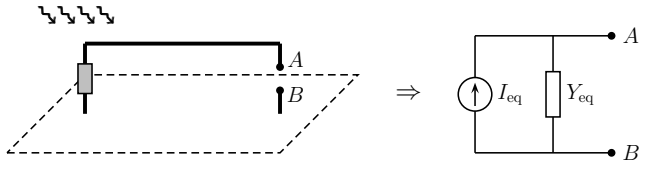

Fig. 6. Casting a field-excited interconnect as a Norton equivalent circuit.

of frequency. Therefore, a rational macromodel is readily obtained using the standard Vector Fitting algorithm [7] (18 poles were automatically determined so that the relative RMS model error resulted less than 1%), followed by a passivity check based on [15] (model was already passive and did not require any a posteriori enforcement).

The equivalent current source $I_{\rm eq}$ is computed by turning on the incident field and replacing Z_L with a short circuit. This current depends both on frequency s and on the incidence angles of the impinging field, thus requiring a parameterized macromodel representation. Figure 7 validates the computed parameterized macromodel of $I_{\rm eq}(s,\eta)$ for fixed $\psi = 0^o$ and $\theta = 45^o$, whereas Figure 8 provides the same validation for $I_{\rm eq}(s,\psi)$ with $\eta = 180^o$ and $\theta = 45^o$. Only a selected number of curves for few angles η_m, ψ_m and a subset of model frequency samples ω_k (red dots) are shown for readability, but similar results were obtained for all angles within the range $[0^o, 360^o]$ and all other frequencies. In both cases, a very good accuracy is observed, with the model responses being almost undistinguishable from the original responses computed by NEC. The (cumulative, relative) model approximation errors

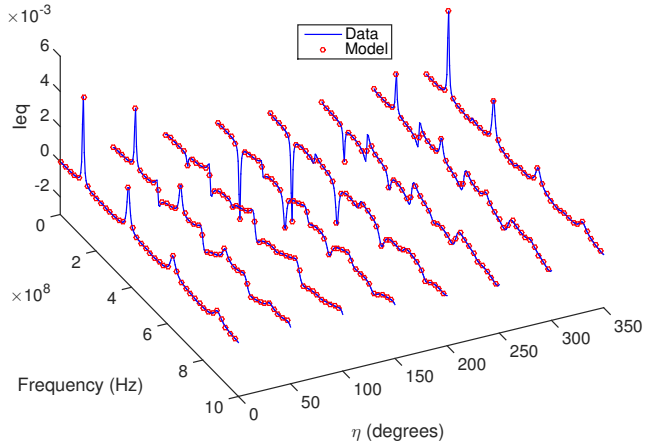

Fig. 7. Macromodel ($N = 20$, $L = 7$) validation of the NEC-based short-circuit current $I_{\rm eq}(s,\eta)$, with $\psi = 0^o$ and $\theta = 45^o$. Cumulative relative macromodel error: $\epsilon = 1.9 \times 10^{-3}$.

are defined as

$$\epsilon = \|\mathbf{E}\|_F / \|\breve{\mathbf{I}}\|_F, \tag{11}$$

with matrices $\mathbf{E}$ and $\breve{\mathbf{I}}$ collecting all frequency and angular samples of data and model according to

$$\breve{I}_{k;m} = \breve{I}_{\rm eq}(\mathrm{j}2\pi f_k; \vartheta_m), \quad E_{k,m} = I_{\rm eq}(\mathrm{j}2\pi f_k; \vartheta_m) - \breve{I}_{k;m}$$

where F denotes the Frobenius norm. We remark that all model orders N, L were determined to achieve a relative error $\epsilon \lesssim 1\%$.

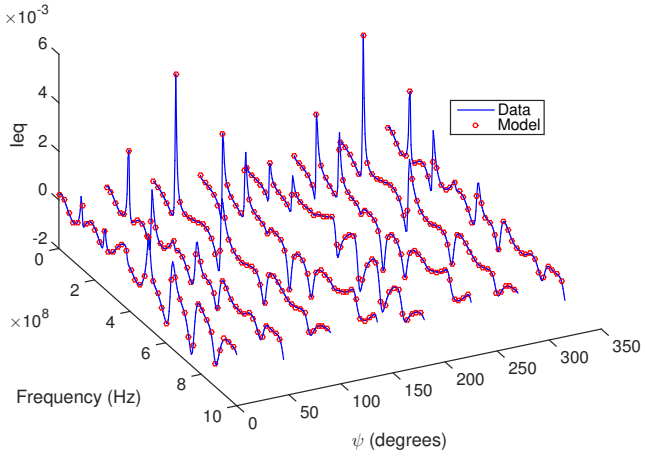

Fig. 8. Macromodel ($N = 40$, $L = 7$) validation of the NEC-based short-circuit current $I_{\rm eq}(s, \psi)$, with $\eta = 180^o$ and $\theta = 45^o$. Cumulative relative macromodel error: $\epsilon = 1.2 \times 10^{-2}$.

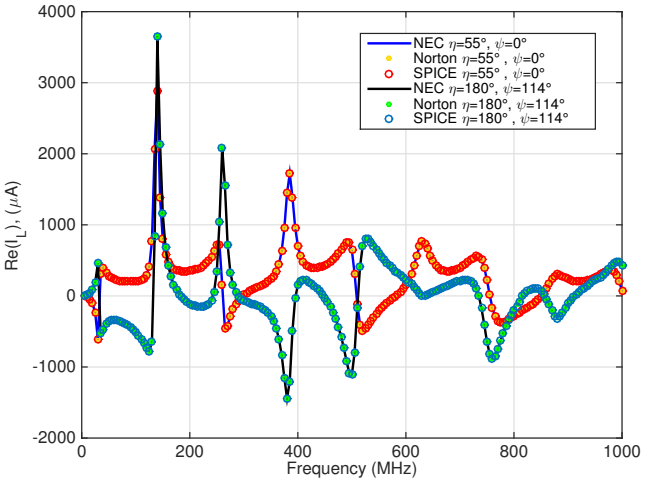

Fig. 9. Validation of the NEC-based parameterized Norton model for the determination of the load current I_L flowing through a RLC load, excited by a normalized incident field $E = 1$ V/m ($\theta = 45^o$).

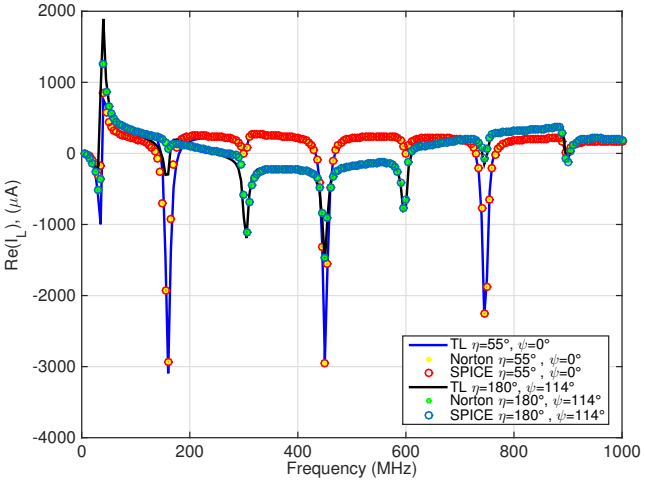

Fig. 10. Validation of the transmission line-based parameterized Norton model for the determination of the load current I_L flowing through a RLC load, excited by a normalized incident field $E = 1$ V/m ($\theta = 45^o$).

A complete validation of the modeling flow is provided in Figure 9, where the load current I_L is computed by solving the parameterized Norton macromodel loaded by a series RLC load ($R = 5\,\Omega$, $L = 10\,$nH, $C = 10\,$pF). The results are compared for few selected angles η and ψ to the reference currents obtained by a direct application of NEC to the loaded structure. Almost no difference is visible in all reported cases (similar results were obtained for all other angle configurations). The figure reports also the SPICE simulation results applied to the parameterized Norton equivalent model, synthesized as an equivalent circuit following [1], [20]. Also this SPICE realization matches closely the reference solution. As an further validation, we repeated the same macromodel identification, but starting from reference frequency responses based on the pure transmission-line coupling model [26] (thus neglecting edge discontinuities, vertical riser and re-radiation effects). The results are depicted in Figure 10. Also in this case the macromodel accuracy is excellent, demonstrating the agnostic nature of proposed macromodeling strategy with respect to the first-principle model used to generated the raw frequency responses. We conclude that the proposed parameterized modeling strategy can be used to represent field-excited interconnect structures through non-homogeneous circuit equivalents, where the equivalent source models are due to incident fields.

A. Transient analysis of field-excited interconnects loaded by nonlinear devices

The SPICE realization of the above-derived parameterized Norton macromodel can be used for transient analysis of the field-excited interconnect, loaded by arbitrary and possibly nonlinear terminations, and for any prescribed time variation of the incident field $e(t)$. We demonstrate this approach by replacing the load impedance Z_L with a nonlinear termination including a series resistor ($R_L = 100\,\Omega$) and a symmetric voltage clipping circuit with two parallel branches, each with two series-connected diodes, and by performing a transient analysis using an incident field waveform $e(t) = E_0 \sin(2\pi f_0 t) u(t)$, with $f_0 = 100$ MHz, $E_0 = 10\,$V/m, and where $u(t)$ is the Heaviside unit step function. Figure 11 compares the load voltage induced by the incident field with or without the clipping circuit, using two different models for the diodes.

B. An application: EMI on a high-speed link

As an additional application, we consider another transmission line structure ($\mathcal{L} = 10$ cm, wire radius $r_w = 0.1$ mm, height $h = 1$ cm over an ideal ground plane), which is modeled as a two-port structure. Both the admittance matrix $\mathbf{Y}_{\rm eq}(\mathrm{j}\omega)$ and the two short-circuit currents $I^{\rm eq}_{1,2}(\mathrm{j}\omega; \alpha)$ parameterized by $\alpha = \psi$ and η (with $\theta = 45^o$) induced by an incident plane wave were computed by NEC, as in previous sections. Then, a parameterized two-port Norton macromodel was computed using the proposed fitting procedure up to 10 GHz and synthesized as a SPICE equivalent.

A typical applicaton that is enabled by the macromodel is demonstrated in Figure 12. The line is driven on one end by a clock signal (voltage swing: 1 V, internal source resistance

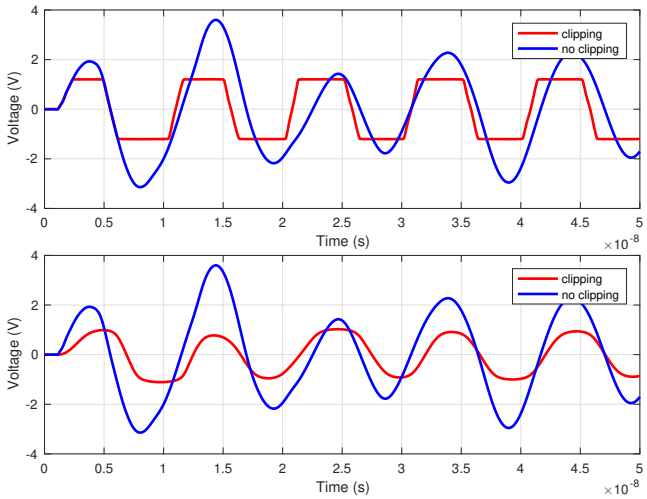

Fig. 11. Transient analysis of the field-excited transmission line terminated by a nonlinear overvoltage protection circuit (top panel: ideal diode model; bottom panel, diode model 1N4148).

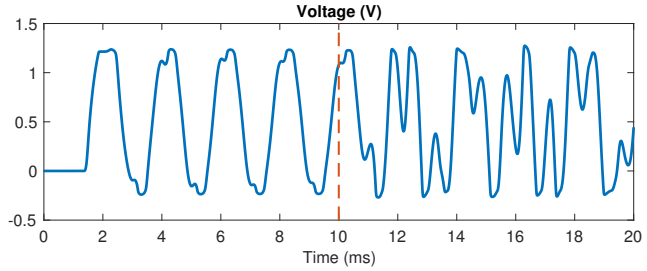

Fig. 12. Transient response of a clock-driven transmission line disturbed by an incident field triggered at $T_* = 10$ ns.

$R_S = 50\,\Omega$, bit time: 1 ns, rise and fall times: 100 ps) and terminated into a parallel RC load ($R_L = 10\,k\Omega$, $C_L = 1$ pF) protected by a diode-based circuit clipping the voltage within the range $[-0.2, 1.2]$ V. A continuous-wave (50 V/m, 1.3 GHz) indicent field from a direction $(\theta, \psi, \eta) = (45^o, 0^o, 55^o)$ is then switched on at $T_* = 10$ ns (red dashed line in the figure). The received voltage at the far end of the line is significantly distorted by the disturbing field, as Figure 12 confirms. The SPICE runtime for this simulation took only 0.19 seconds on a standard laptop.

VII. Mode Tracking in Reverberation Chambers

We now discuss a different application scenario for the proposed Fourier-rational parameterized macromodels. We refer to a generic reverberation chamber depicted in Fig. 2, whose scattering responses $\mathbf{S}(s;\theta)$ measured by a pair of antennas are parameterized by the stirrer rotation angle θ. The main objective is here to identify from direct measurements all the natural frequencies of the chamber within a given frequency band. Such frequencies can be identified from the set of poles $p_i(\theta)$ of a rational approximation. Such poles inherit the dependence on θ and are therefore easily computed from our proposed Fourier-rational macromodel.

We illustrate the proposed pole identification and extraction on the chaotic reverberation chamber discussed in [2], namely

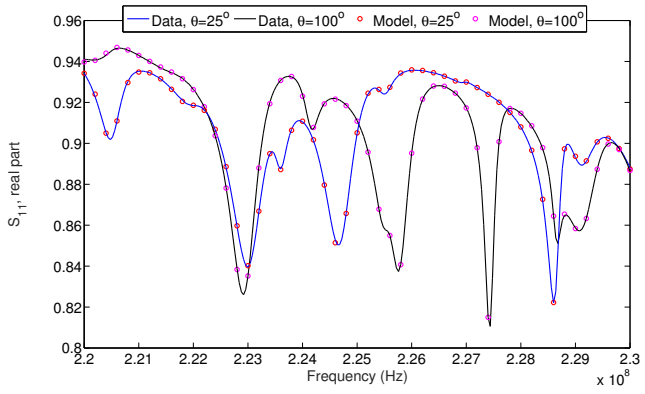

Fig. 13. Comparison between parameterized macromodel and measured scattering responses of the reverberation chamber.

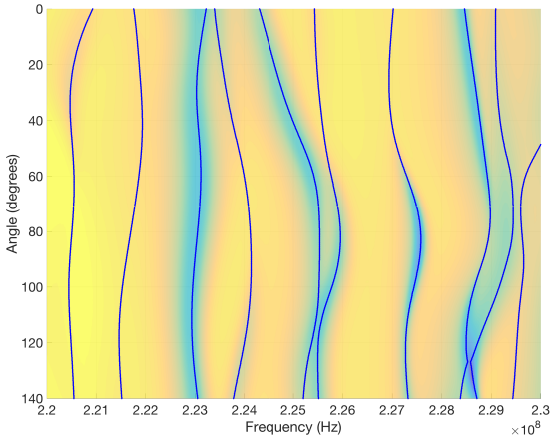

Fig. 14. Pole trajectories (imaginary parts, blue dots) superimposed to $|\breve{S}_{11}(2\pi f, \theta)|$ rendered with a linear color scale (ranging from dark blue to yellow).

a cubic metallic cavity (size $w = 2.95$ m, $l = 2.75$ m, $h = 2.35$ m) equipped by a stirrer and with six defocusing hemispheres (radius 0.4 m) attached to the chamber walls. The frequency band of interest for this investigation ranges from $f_{\min} = 220$ MHz to $f_{\max} = 230$ MHz, which is slightly below the Lowest Useable Frequency (LUF) of the chamber (around 300 MHz). The 2×2 scattering matrix $\breve{\mathbf{H}}_{k;m} = \breve{\mathbf{S}}(\mathrm{j}2\pi f_k; \theta_m)$ in (1) was measured in one-degree steps over the stirrer rotation range $[0^o, 140^o]$, obtaining a total number of frequency samples $K = 501$ for each angle ($M = 141$). The construction of the macromodel was performed using all K frequency samples for a subset of $M' = 29$ angular samples (one point out of five), whereas the remaining angular samples were used as validation points for checking the intersample approximation. The rational model order and the Fourier model order was increased until the accuracy of the approximation was satisfactory and finally set to $N = 24$ and $L = 3$ (higher orders did not improve significantly the fitting accuracy).

Figure 13 compares few selected scattering responses of the parameterized macromodel to the corresponding raw measured data. We see that the accuracy of the approximation is

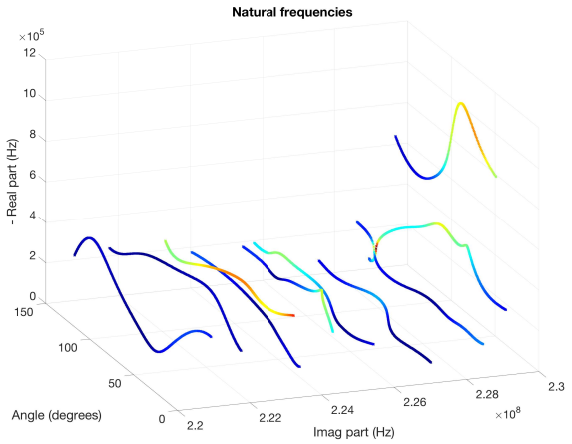

Fig. 15. Pole trajectories (both real and imaginary parts) parameterized by stirrer position. The colors represent the residue magnitude associated to each pole, using a normalized colorscale ranging from blue to red.

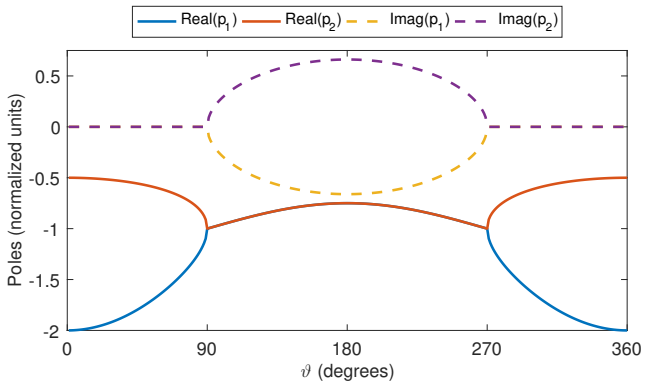

Fig. 16. Trajectory of the two roots of $\mathsf{k}(s,\vartheta)$ in (12).

excellent. Figure 14 reports the trajectory of the macromodel poles (imaginary part) versus stirrer rotation angle. The pole trajectories are superimposed to a colored map of the insertion loss magnitude (same color scale as in Fig. 5), in order to confirm that the pole trajectories closely match the peaks of the frequency responses. Finally, a 3D plot of the poles (both real and imaginary parts) plotted versus rotation angle is reported in Figure 15, where different colors are used to represent the magnitude of the residues associated to each pole, for each stirrer position. Thus, the color can be used to indirectly infer the field strength of the corresponding resonant mode at the excitation and measurement locations, which is of course dependent on the type, orientation, and location of the measuring antennas, in addition to the field topography of the mode. From this figure, we note that the highest-frequency pole trajectory falls partly outside the bandwidth of interest and should be disregarded (see also Figure 14), since its precise identification would require the missing frequency samples above 230 MHz.

Overall, these results confirm a very good confidence in the correctness of the estimated natural frequencies of the chamber. Therefore, it is expected that this pole extraction methodology will lead to significant improvements in building statistical distributions of resonances from direct measurements, with respect to existing more consolidated methods [28], [29], which perform pole extraction independently for each different stirrer position. This investigation is in progress and will be documented in a future report.

VIII. Conclusions

This paper proposed a Fourier-rational macromodel structure and a relatated parameter identification algorithm based on a reformulation of the Sanathanan-Koerner iteration. This model structure is a natural choice for compact dynamical modeling of linear electromagnetic systems, whose responses depend on periodic geometrical parameters. Both model structure and identification have been validated on a low-order circuit example. In addition, two possible application scenarios have been discussed: a field-excited interconnect, for which a parameterized SPICE equivalent was derived based on either a transmission-line or a full-wave model, and a reverberation chamber, whose natural frequencies dependence on stirrer rotation angle have been identified from direct mesurements. These two examples were selected due to their relevance for the EMC community. However, the presented macromodeling strategy is general and can be applied in principle to any linear (or linearized) system with periodic parameters.

IX. Acknowledgements

The Authors would like to thank Prof. Elodie Richalot (ESYCOM Lab, Université Paris-Est Marne-la-Vallée, France) for carrying out and sharing the S-parameter Reverberation Chamber measurements that were analyzed in Section VII.

Appendix

Consider the second-order polynomial

$$\mathsf{k}(s,\vartheta) = s^2 + (2 + 1/2\cos(\vartheta))s + 1 \qquad (12)$$

Figure 16 shows the trajectory of the two roots $p_{1,2}(\vartheta)$ of $\mathsf{k}(s,\vartheta)$ as functions of the parameter ϑ. The figure clearly shows that both real and imaginary parts of $p_{1,2}(\vartheta)$ are non-smooth functions of ϑ, due to the presence of two bifurcation points where switching between a real-only to a complex conjugate pair occurs. This simple example shows that a direct parameterization of the poles or zeros of a parameter-dependent frequency response in terms of smooth basis functions is not appropriate.

Let us define the two auxiliary poles $q_{1,2} = p_{1,2}(0)$, i.e., $q_1 = -2$ and $q_2 = -1/2$. A straightforward derivation leads to the identity

$$\frac{\mathsf{k}(s,\vartheta)}{(s+q_1)(s+q_2)} = 1 + \frac{2(1+\cos(\vartheta))/3}{s+q_1} - \frac{(1+\cos(\vartheta)/6}{s+q_2}$$

where the right-hand side matches the format of the denominator $\mathsf{D}(s,\vartheta)$ in the proposed model formulation (3). The three terms correspond to three frequency-dependent basis functions $\varphi_n(s)$ of (5) for $n = 0, 1, 2$. Only two Fourier basis

functions $\xi_\ell(\vartheta)$ with $\ell = 0, 1$ are required in this case, with the corresponding coefficients reading

$$d_{0,0} = 1 \qquad d_{0,1} = 2/3 \qquad d_{0,2} = -1/6$$
$$d_{1,0} = 0 \qquad d_{1,1} = 2/3 \qquad d_{1,2} = -1/6$$

This example confirms that the adopted model representation (3) is able to represent non-smooth poles behavior through a smooth implicit parameterization, here based on the Fourier basis (4).

REFERENCES

[1] S. Grivet-Talocia and B. Gustavsen, *Passive Macromodeling: Theory and Applications*. New York: John Wiley and Sons, 2016.

[2] E. Richalot, U. Kuhl, O. Legrand, F. Mortessagne, J. B. Gros and S. Grivet-Talocia, "Experimental characterization of the distribution of resonance widths in chaotic reverberation chambers," 3rd IEEE International Workshop on Metrology for Aerospace, Florence, Italy, 21–23 June 2016, pp. 177–181.

[3] A.C. Antoulas, *Approximation of large-scale dynamical systems*, SIAM, Philadelphia, 2005.

[4] W.H.A. Schilders, H.A. Van Der Vorst, and J. Rommes, *Model order reduction: theory, research aspects and applications*, Springer Verlag, 2008.

[5] M. Nakhla and R. Achar, "Simulation of High-Speed Interconnects", *Proc. IEEE*, May 2001, Vol. 89, No. 5, pp. 693–728.

[6] M. Celik, L. Pileggi, A. Odabasioglu, *IC Interconnect Analysis*, Springer, 2002.

[7] B. Gustavsen, A. Semlyen, "Rational approximation of frequency domain responses by vector fitting", *IEEE Trans. Power Del.*, vol. 14, no. 3, pp. 1052-1061, July, 1999.

[8] D. Deschrijver, B. Haegeman, T. Dhaene, "Orthonormal Vector Fitting: A Robust Macromodeling Tool for Rational Approximation of Frequency Domain Responses," *IEEE Trans. Adv. Packaging*, vol. 30, pp. 216–225, May 2007.

[9] S. Grivet-Talocia, "Package macromodeling via Time-Domain Vector Fitting," *IEEE Microwave Wireless Comp. Lett.*, Vol. 13, No. 11, 2003.

[10] D. Deschrijver, M. Mrozowski, T. Dhaene, D. De Zutter, "Macromodeling of Multiport Systems Using a Fast Implementation of the Vector Fitting Method," *IEEE Microwave and Wireless Components Letters*, Vol. 18, N. 6, June 2008, pp.383–385.

[11] Mayo, A. J. & Antoulas, A. C. (2007). A framework for the solution of the generalized realization problem. *Linear Algebra and Its Applications*, 405(2-3), 634–662.

[12] Z. Qi, H. Yu, P. Liu, S.X.Tan, L. He, "Wideband passive multiport model order reduction and realization of RLCM circuits," *IEEE Trans. on Computer-Aided Design of Integrated Circuits and Systems*, vol. 25, no. 8, pp. 1496–1509, Aug. 2006

[13] G. Antonini, "SPICE equivalent circuits of frequency-domain responses," *IEEE Trans. on Electromagnetic Compatibility*, vol. 45, no. 3, pp. 502–512, Aug. 2003

[14] P. Triverio, S. Grivet-Talocia, M.S. Nakhla, F. Canavero, R. Achar, "Stability, causality, and passivity in electrical interconnect models", *IEEE Trans. on Advanced Packaging*, vol. 30, no. 4, pp. 795-808, 2007.

[15] S. Grivet-Talocia, "Passivity Enforcement via Perturbation of Hamiltonian Matrices" , in *IEEE Trans. Circuits and Systems I: Fundamental Theory and Applications*, pp. 1755-1769, vol. 51, n. 9, September, 2004.

[16] D. Saraswat, R. Achar and M. Nakhla, "Global Passivity Enforcement Algorithm for Macromodels of Interconnect Subnetworks Characterized by Tabulated Data", *IEEE Transactions on VLSI Systems*, Vol. 13, No. 7, pp. 819–832, July 2005.

[17] B. Gustavsen, A. Semlyen, "Enforcing passivity for admittance matrices approximated by rational functions", *IEEE Trans. Power Systems*, Vol. 16, N. 1, pp. 97–104, Feb. 2001.

[18] S. Grivet-Talocia and A. Ubolli, "A comparative study of passivity enforcement schemes for linear lumped macromodels," *IEEE Trans. Advanced Packaging*, vol. 31, pp. 673–683, Nov 2008.

[19] S. Grivet-Talocia, S. Acquadro, M. Bandinu, F. G. Canavero, I. Kelander, and M. Rouvala, "A parameterization scheme for lossy transmission line macromodels with application to high speed interconnects in mobile devices," *IEEE Trans. Electromagnetic Compatibility*, vol. 49, no. 1, pp. 18–24, Feb. 2007.

[20] P. Triverio, S. Grivet-Talocia, and M.S. Nakhla, "A Parameterized Macromodeling Strategy with Uniform Stability Test," *IEEE Transactions on Advanced Packaging*, vol. 32, no. 1, pp. 205-215, Feb. 2009.

[21] E. R. Samuel, L. Knockaert, F. Ferranti, and T. Dhaene, "Guaranteed Passive Parameterized Macromodeling by Using Sylvester State-Space Realizations", *IEEE Transactions on Microwave Theory and Techniques*, vol. 61, no. 4, pp. 1444-1454, Mar. 2013.

[22] F. Ferranti, L. Knockaert, and T. Dhaene, "Passivity-Preserving Parametric Macromodeling by Means of Scaled and Shifted State-Space Systems," *IEEE Transactions on Microwave Theory and Techniques*, vol. 59, no. 10, pp. 2394–2403, Oct. 2011.

[23] F. Ferranti, L. Knockaert, T. Dhaene, "Guaranteed Passive Parameterized Admittance-Based Macromodeling," *IEEE Transactions on Advanced Packaging*, vol. 33, no. 3, pp. 623–629, Aug. 2010.

[24] C. K. Sanathanan and J. Koerner, "Transfer function synthesis as a ratio of two complex polynomials," *IEEE Trans. Automatic Control*, vol. 8, no. 1, pp. 56–58, Jan. 1963.

[25] A. Chinea, S. Grivet-Talocia, H. Hu, P. Triverio, D. Kaller, C. Siviero, and M. Kindscher, Signal integrity verification of multichip links using passive channel macromodels, *IEEE Transactions on Components, Packaging, and Manufacturing Technology*, vol. 1, pp. 920933, June 2011

[26] C. R. Paul, *Analysis of Multiconductor Transmission Lines*, John Wiley and Sons, NY, 1994.

[27] NEC-Win Pro User's Manual, ©1997, Nittany Scientific, Inc., Airline Highway, Hollister, CA 95023–5621.

[28] E. Richalot, K. Selemani, J. B. Gros, O. Picon, O. Legrand, S. Grivet-Talocia, and F. Mortessagne, "Criterion based on resonant frequencies distributions for reverberation chamber characterization," in *Electromagnetics in Advanced Applications (ICEAA), 2015 International Conference on*, Sept 2015, pp. 1112–1115.

[29] U. Kuhl, R. Höhmann, J. Main, and H.-J. Stöckmann, "Resonance widths in open microwave cavities studied by harmonic inversion," *Physical Review Letters*, vol. 100, 2008

[30] C. Yang, H.-D. Brüns, P. Liu, C. Schuster, "Impulse Response Optimization of Band-Limited Frequency Data for Hybrid Field-Circuit Simulation of Large-Scale Energy-Selective Diode Grids," *IEEE Transactions on Electromagnetic Compatibility*, Vol. 58, No. 4 (2016).

[31] I.-T. Chiang et al., "Fast Real-Time Convolution Algorithm for Microwave Multiport Networks With Nonlinear Terminations," *IEEE Transactions on Circuits and Systems – II: Express Briefs*, Vol. 52 (2005).

[32] S. A. Pignari and D. Bellan, "Incorporating vertical risers in the transmission line equations with external sources," in *2004 International Symposium on Electromagnetic Compatibility, Santa Clara, USA; 9-13 August 2004*, pp. 974-979, vol.3.

[33] A. Maffucci, G. Miano and F. Villone, "An enhanced transmission line model for conducting wires," in *IEEE Transactions on Electromagnetic Compatibility*, vol. 46, no. 4, pp. 512-528, Nov. 2004.

[34] Tie Jun Cui and Weng Cho Chew, "A full-wave model of wire structures with arbitrary cross sections," in *IEEE Transactions on Electromagnetic Compatibility*, vol. 45, no. 4, pp. 626-635, Nov. 2003.

[35] F. Rachidi, "A Review of Field-to-Transmission Line Coupling Models With Special Emphasis to Lightning-Induced Voltages on Overhead Lines," in *IEEE Transactions on Electromagnetic Compatibility*, vol. 54, no. 4, pp. 898-911, Aug. 2012.

[36] J. B. Nitsch and S. V. Tkachenko, "Complex-valued transmission-line parameters and their relation to the radiation resistance," in *IEEE Transactions on Electromagnetic Compatibility*, vol. 46, no. 3, pp. 477-487, Aug. 2004.

[37] S. Tkatchenko, F. Rachidi and M. Ianoz, "Electromagnetic field coupling to a line of finite length: theory and fast iterative solutions in frequency and time domains," in *IEEE Transactions on Electromagnetic Compatibility*, vol. 37, no. 4, pp. 509-518, Nov 1995.

[38] S. Lefteriu and A. C. Antoulas, "On the Convergence of the Vector-Fitting Algorithm," in *IEEE Transactions on Microwave Theory and Techniques*, vol. 61, no. 4, pp. 1435-1443, April 2013.

[39] G. Shi, "On the Nonconvergence of the Vector Fitting Algorithm," in *IEEE Transactions on Circuits and Systems II: Express Briefs*, vol. 63, no. 8, pp. 718-722, Aug. 2016.

Stefano Grivet-Talocia (M'98–SM'07) received the Laurea and the Ph.D. degrees in Electronic Engineering from Politecnico di Torino, Italy. From 1994 to 1996, he was with the NASA/Goddard Space Flight Center, Greenbelt, MD, USA. Currently, he is a Full Professor of Electrical Engineering with Politecnico di Torino. His research interests are in passive macromodeling of lumped and distributed interconnect structures, model order reduction, modeling and simulation of fields, circuits, and their interaction, wavelets, time-frequency transforms, and their applications. He is author of more than 150 journal and conference papers. He is co-recipient of the 2007 Best Paper Award of the IEEE Trans. Advanced Packaging. He received the IBM Shared University Research (SUR) Award in 2007, 2008 and 2009. Dr. Grivet-Talocia served as Associate Editor for the IEEE TRANSACTIONS ON ELECTROMAGNETIC COMPATIBILITY from 1999 to 2001. He co-founded the academic spinoff company IdemWorks in 2007, serving as President until its acquisition by CST in 2016.

Elisa Fevola received the B.Sc. degree in Electronic Engineering in 2016, from Politecnico di Torino, Turin, Italy, where She is currently pursuing the M.Sc. in Electronic Engineering. Her current research interests are in electromagnetic and circuit simulation, with emphasis on passive and parameterized reduced order modeling.